Dynamics and structure of an aging binary colloidal glass

Jennifer M. Lynch, Gianguido C. Cianci, and Eric R. Weeks[*]

Department of Physics, Emory University, Atlanta, Georgia 30322, USA

(Received 3 July 2008; revised manuscript received 23 August 2008; published 30 September 2008)

We study aging in a colloidal suspension consisting of micron-sized particles in a liquid. This system is made glassy by increasing the particle concentration. We observe samples composed of particles of two sizes, with a size ratio of 1:2.1 and a volume fraction ratio 1:6, using fast laser scanning confocal microscopy. This technique yields real-time, three-dimensional movies deep inside the colloidal glass. Specifically, we look at how the size, motion, and structural organization of the particles relate to the overall aging of the glass. Particles move in spatially heterogeneous cooperative groups. These mobile regions tend to be richer in small particles, and these small particles facilitate the motion of nearby particles of both sizes.

I. INTRODUCTION

A liquid can be crystallized by slowly lowering its temperature below T_m, the crystal melting temperature. On the other hand a rapid temperature quench to below T_g, the glass transition temperature, yields an amorphous solid with interesting nonequilibrium properties [1–7]. More specifically, the glassy dynamics slow down dramatically and do so on macroscopically large time scales. This phenomenon is known as aging and has been seen in a variety of glass-forming materials [7–20]. However, the microscopic mechanisms by which a system ages are still unclear [21].

Dense colloidal suspensions are good models to study glassy systems. These are composed of small micron-sized solid particles in a liquid. In these systems, the glass transition is reached by increasing the volume fraction, and a glass is formed once the volume fraction is greater than $\phi_g \approx 0.58$ [22]. Previous work looked at aging in colloidal glasses composed of particles of one size [10,23]. A small (5%) size polydispersity was used to inhibit crystallization on experimental time scales [24,25]. In this paper, we study aging in a binary colloidal system. To an extent the binary system facilitates comparison with prior simulations [26,27], but our larger size ratio (2.1:1) also highlights the role of the different sizes in the aging process.

In particular, we find that smaller particles are more mobile than expected. These significantly larger movements are key components of the aging process since, in our system, the structural arrangement of the colloidal particles completely determines the "age" [10]. Particles moving to new positions change the structure and allow the system to become "older." Thus, we conjecture that the small, unusually mobile particles are a key component of the aging process, and perhaps facilitate other, more subtle structural changes of the slower moving large particles [28–30]. This is reflected in the tendency for the neighbors of small particles to have higher mobility on average, and gives insight into the structural origin of the aging process.

II. EXPERIMENTAL METHODS

We use two sizes of poly(methyl methacrylate) (PMMA) particles that are dyed with rhodamine 6G [31,32], as shown in Fig. 1. These particles are suspended in a mixture of 85% cyclohexylbromide and 15% decalin by weight. This mixture closely matches both the density and refractive index of the particles [31]. The small particles have a radius of $a_S = 0.56 \pm 0.05$ μm and the large particles have a radius of $a_L = 1.17 \pm 0.05$ μm; the error bars reflect the uncertainty of the mean radius of each particle species, and additionally each species has a polydispersity of ~5%. The number ratio of small to large particles is 1.48:1, but given the large size ratio 1:2.1, the volume fraction ratio is 1:6. The total volume fraction is $\phi_{S+L} \approx 0.62$. We do not see any demixing of the two colloidal species, perhaps because the sample is glassy and thus particle motion is difficult.

In individual monodisperse samples, the two particle species would each be expected to have a glass transition at $\phi_g \approx 0.58$. For volume fractions slightly less than ϕ_g, a monodisperse sample should form crystals in a finite time, and for samples with volume fractions slightly above ϕ_g, previous colloidal samples similar to ours only find crystals which nucleate at flat boundaries and which only grow into the bulk of the sample a short distance [22,33,34]. It is the lack of homogeneous crystal nucleation that is used to define ϕ_g for these monodisperse samples, although in practice it is probable that a slight polydispersity of the particles is needed
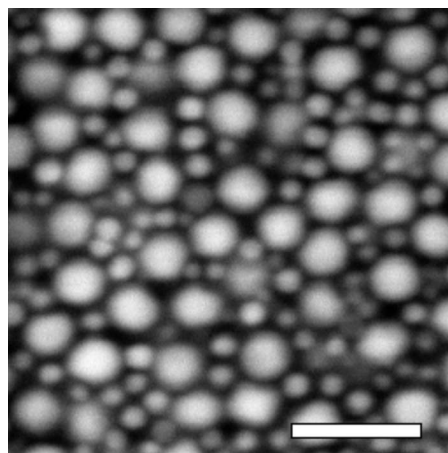

FIG. 1. Confocal micrograph of the binary colloidal glass studied in this experiment. The image was taken 20 μm inside the sample. The scale bar represents 5 μm.

*weeks@physics.emory.edu

to truly prevent crystallization [34,35]. Given that the two monodisperse colloidal samples should have the same ϕ_g, it is worth noting that our binary sample is not analogous to mixtures of two polymer glasses with different glass transition temperatures T_g, which are known to have interesting behaviors [36,37]. In practice, for our sample, we cannot use the lack of crystallization to define ϕ_g as our binary sample does not crystallize at any volume fraction. Instead, we regard our sample as glassy as the dynamics do not equilibrate, but change with age for as long as we have observed, as will be discussed in detail in Sec. III.

We use fast laser scanning confocal microscopy which yields clear images deep inside our dense samples [38]. Despite the high density, the two colloidal species can be easily discerned. We acquire three-dimensional (3D) scans of our sample yielding a $53 \times 53 \times 15$ μm^3 observation volume. The acquisition time for one 3D image (~ 8 s) is several orders of magnitude faster than the diffusion time for the particles at this volume fraction. We continuously follow the sample's aging over 1.5 h at a rate of three images per minute. This allows us to track ~ 5000 particles in three dimensions over the course of the experiment [31,39].

To study aging, we first must initialize aging in the sample. There are two approaches to initialization in any glassy system [40]. The first is to quench a sample from a liquid state. In a conventional glass, this is done by rapidly lowering the temperature or increasing the pressure. In a hard sphere or colloidal glass, this would be done by starting with a sample with a volume fraction $\phi < \phi_g$ and then rapidly increase the volume fraction to above ϕ_g. Currently, there is no experimental technique that allows for this method in a sample of hard PMMA colloids. The second method for initializing aging involves shear rejuvenation: By applying a large shear to a system (above any yield stress), in some cases the aging appears to be reinitialized. This is the method used in this study and previous studies on aging with colloids [10,23,41–43]. There are questions as to whether these two methods lead to the same glass [40], but for our current study, we stress that only the second of these methods is experimentally available. Experimentally, this leads to a reproducible initial state [23] and the dynamics appear similar to a conventional glass aging via a rapid quench from a liquid state, as will be shown below.

To shear rejuvenate the sample, we begin each experiment by pulling a small metal wire that is present in the samples with a hand held magnet, thus shear melting the glass and re-initializing the aging process. We begin taking data, and thus define our initial time $t_w = 0$, within 20 s after we finish pulling the wire. In practice, transient flows continue for a few seconds after cessation of the stirring, and these flows likely still shear the glass, resulting in some uncertainty of the initial time. However, the 20 s delay between ending the stirring and starting the data acquisition is long enough to allow for these flows to decrease quite significantly, and we see no signs of shearing even at the start of data acquisition. Thus, there is at most an uncertainty of 20 s for our choice of $t_w = 0$, and in practice the results shown in this work are for time scales much longer than 20 s.

TABLE I. We divide the data into five temporal windows, each window beginning at $t_w = t_1$ and ending at $t_w = t_2$, with values t_1 and t_2 listed below. For each window, $t_2 = 1.7 t_1$ and the "age" $\bar{t}_w$ is defined as the geometric mean of t_1 and t_2. All times are in minutes.

$\bar{t}_w$	t_1	t_2
8.7	6.7	11.3
15	11.3	20
26	20	34
45	34	58
76	58	100

III. RESULTS

Aging in glasses is defined as the dependence of the dynamical properties of the system on the time elapsed since vitrification. To quantify these changing dynamics, we calculate the mean-squared displacement (MSD), defining displacements $\Delta \vec{r}_i(t_w, \Delta t) = \vec{r}(t_w + \Delta t) - \vec{r}(t_w)$, and the MSD as $\langle \Delta r^2 \rangle_{i,t_w}$. The angle brackets indicate an average over all particles i (of a given particle size), and over all times t_w; the MSD is thus a function of the lag time Δt. In practice, we wish to understand the t_w dependence of the MSD as well. Thus, while we continuously take data for 1.5 h, we divide the data into five temporal windows, and calculate the MSD restricting the average over times t_w within each window. The windows are formed logarithmically based on the sample age t_w and each temporal window is characterized by its geometric mean age $\bar{t}_w$; see Table I for details. For each window, the MSD is calculated for lag times Δt up to $\sim 0.5 \bar{t}_w$, and it is important to recognize that for the largest lag times in each window, the data are aging during the observation window. Thus, care must be taken in interpreting the MSD curves. Nonetheless, this method provides a way to characterize the dynamics for a given age $\bar{t}_w$.

Figure 2 shows the MSDs of the glass over a total period of 1.5 h for the large and small particles. At short time scales, the motion of a particle is expected to be diffusive as
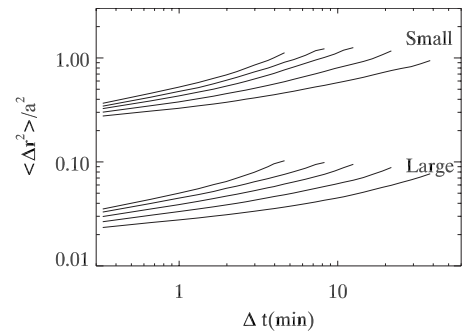

FIG. 2. Aging mean-squared displacement for large and small particles of a binary colloidal glass at $\phi \approx 0.62$. The five curves represent five different ages of the sample. The geometric mean ages of the curves, from top to bottom, are $\bar{t}_w = 8.7$, 15, 26, 45, and 76 min; see Table I for details. The mean-square displacements are normalized relative to each particle size, that is, for the small particles we plot $\langle \Delta r^2 \rangle / a_S^2$ and for the large particles we plot $\langle \Delta r^2 \rangle / a_L^2$.

each particle explores its local environment without noticing its neighbors. However, at these high densities, particles are crowded, and this diffusive regime can only be observed on time scales shorter than our image acquisition rate and is therefore not visible in Fig. 2. Instead, we observe a plateau for most of our time scales, indicating that a particle's motion is slower and more inhibited than normal diffusion. This is because particles are trapped in cages formed by their neighbors [44]. At long time scales, the MSDs show an upturn, with the time scale of this upturn increasing with the age of the sample.

Both the large and small particles' dynamics are aging similarly, showing upturns at similar lag times. Clearly in our experiments, the aging of each species is strongly coupled to that of the other. Were we comparing two monodisperse samples with different particle sizes a_S and a_L, the horizontal axis of Fig. 2 would need to be rescaled by the diffusion time scale for each particle, $\tau_D = 3\pi\eta a^3/k_B T$, where η is the solvent viscosity, k_B is Boltzmann's constant, and T is the absolute temperature. τ_D thus depends sensitively on particle radius a, and the ratio of diffusion time scales for our particle sizes is $(a_L/a_S)^3 \approx 9$. However, in our data, clearly the upturns in the MSD curves occur at quite similar time scales (Fig. 2), rather than differing by an order of magnitude. These essentially similar upturns indicate the system has a single time scale for structural rearrangements of both species, and this time scale grows as the sample ages. As noted in Sec. II, this is perhaps reasonable for a binary colloidal mixture but stands in contrast to mixtures of polymers with differing glass transition temperatures [36,37]. In fact, it suggests that in our experiment the relevant time scale determining structural rearrangements is $\bar{t}_w$ (which is the same for both species) and not the diffusion time scale τ_D (which differs by a factor of 9).

In Fig. 2 we nondimensionalized $\langle \Delta r^2 \rangle$ to better compare the behavior of large and small colloids. The height of the plateau of the MSD curve is related to the cage size [44], which would be the same nondimensional size for two monodisperse samples. In our binary sample, we observe the nondimensional cage size is larger for small particles. For example, at $\bar{t}_w = 76$ min and using a time scale $\Delta t = 10$ min, we find $(\langle \Delta r_L^2 \rangle)^{1/2} = 0.25$ μm$=0.21a_L$, and $(\langle \Delta r_S^2 \rangle)^{1/2} = 0.43$ μm$=0.76a_S$. Thus, the small particles are more mobile in their cages, both in an absolute sense, and especially so when taking into account their smaller size.

A further way to characterize the dynamics is to examine the self-intermediate scattering function for the two species. This is calculated as

$$F_s(\vec{k}, \Delta t) = \langle \exp(-i\vec{k} \cdot \Delta \vec{r}_i) \rangle_{i,t_w}, \tag{1}$$

where the angle brackets again indicate an average over starting times t_w and over all particles of a given size, similar to the definition of the mean-square displacement. In practice, we choose $|\vec{k}|$ from the maximum of the static structure factor for each species, and additionally we average over orientations of $\vec{k}$. The results are shown for the five time windows in Fig. 3. $F_s(\Delta t)$ has a downturn for both species around similar values of Δt for each age $\bar{t}_w$. The overall
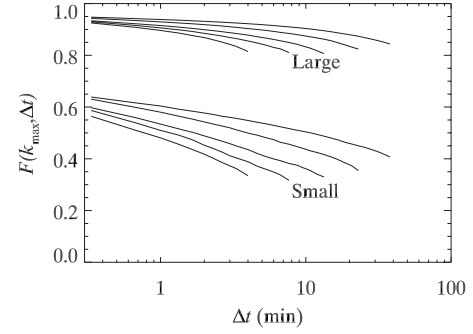

FIG. 3. Self-intermediate scattering function for each particle species. Each group of five curves represent five different ages of the sample. The geometric mean ages of the curves, from bottom to top, are $\bar{t}_w = 8.7$, 15, 26, 45, and 76 min; see Table I for details. Each scattering function is computed for the wave vector k_{max} which maximizes the structure factor for that particle species. The specific values are $k_{max} = 5.61$ μm^{-1} for the small particles and $k_{max} = 3.14$ μm^{-1} for the large particles.

magnitude of $F_s(\Delta t)$ is larger for the large particles, reflecting that they move less, as shown in Fig. 2. Thus, the two particle sizes clearly have different albeit connected dynamics. As with the MSD curves, note that at the largest time scales Δt shown in Fig. 3, the sample is aging over that time scale. Given that the sample ages before complete decay can be seen, it is difficult to characterize the decay of $F_s(\Delta t)$, but we note that the downturn seen at longer lag times is linked to the small irreversible structural rearrangements of the sample.

We wish to investigate the relationship between structure and dynamics, that is, how a particle's local environment influences its motion and the motion of its neighbors [10,23]. Prior work indicated that the particles rearrange in cooperative groups [23], similar to what is seen in supercooled liquids [3,33,45–51] and granular materials [52,53]. A starting point to look for cooperativity is to ask where the mobile particles are located [23,46,49]; Fig. 4 highlights the most mobile particles at $t_w = 20$ min, using $\Delta t = 10$ min. The color-
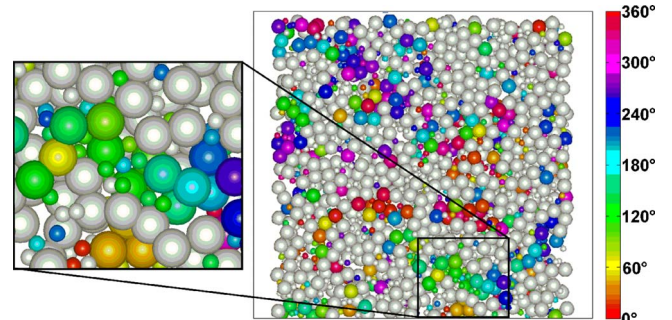

FIG. 4. (Color online) A narrow slice of a three-dimensional sample with width $\Delta z = 4$ μm at $t_w = 20$ min. Particles with the 30% greatest displacements $\langle \Delta r \rangle \geqslant 0.375$ μm for $\Delta t = 10$ min are colored with color indicating the direction of displacement projected onto the xy plane, where 0° indicates motion to the right and 90° indicates motion directly upwards. When viewed in grayscale, lighter shades indicate motion upwards, and darker shades indicate motion downwards.
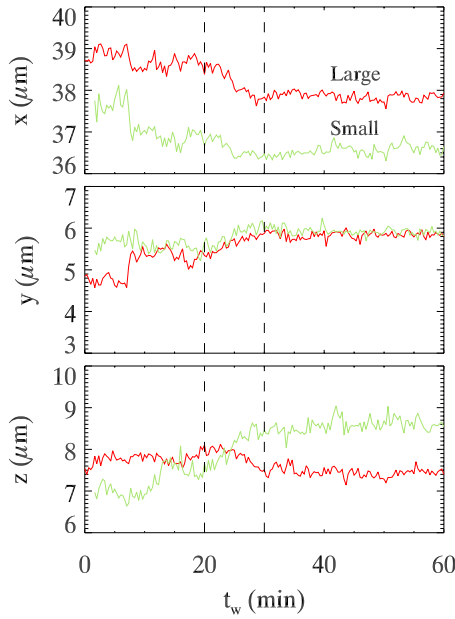
FIG. 5. (Color online) Trajectories of two neighboring particles: A large particle [(red) dark gray] and a small particle [(green) light gray]. The particles have large displacements at $t_w=20$ min, using $\Delta t=10$ min. The vertical dashed lines indicate this time range $t_w, t_w+\Delta t$.

ing indicates the direction of motion. Several features are seen. First, mobile particles are clustered, as was reported in monodisperse samples [23]. A mobile particle is likely to have mobile neighbors. Second, particles of similar colors are likely to be neighbors, indicating that groups of mobile particles are moving in similar directions. For example, the magnified region in Fig. 4 shows a group of particles all moving approximately up and to the left (green and blue colors). Third, occasionally neighboring particles have significantly different directions of motion, similar to the "mixing" particles seen in supercooled fluids [44]. This tendency is enhanced for the small species, which can often move in directions different from their larger neighbors. These three observations highlight that indeed the motion of a particle is related to the motion of its neighbors, as discussed before. It is these cooperative motions that are responsible for the upturn in the MSD curves (Fig. 2).

The trajectories of two mobile particles are shown in Fig. 5, further demonstrating the cooperative motion. These are neighboring particles taken from those shown in Fig. 4. One is a large particle [(red) dark gray] and the other is small [(green) light gray]. At $t_w=20$ min they both begin to move in similar directions, with the motion essentially complete by $t_w=30$ min. Subsequent to the rearrangement, these two particles remain caged for the next 30 minutes (further data not shown). Figure 5 shows that these large displacements happen slowly in our aging glass; while the particles each move ~ 1 μm, this takes the whole time interval $\Delta t=10$ min. Occasionally some particles move more rapidly, and some move more slowly; similar results to Fig. 4 can be seen using other choices of Δt, and indeed motions of other durations can be seen in the trajectories of Fig. 5 at other times.

These observations do not yet show how the local structural environment influences the motion. To quantify the
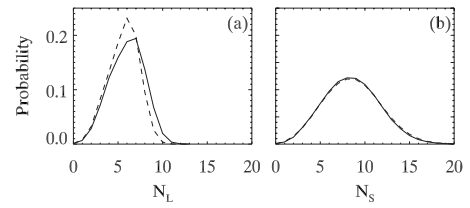

FIG. 6. Probability of a large particle (solid line) and a small particle (dashed line) having a certain number of (a) large neighbors and a certain number of (b) small neighbors. These distributions do not change as the sample ages.

structure of the local environment of a particle, in Fig. 6 we plot the probability of a particle having N_L large neighbors (a) or N_S small neighbors (b). The probabilities are computed separately for large and small reference particles. We define a neighbor as a particle within 2.8 μm from the reference particle being considered. This cutoff distance is set by the first minimum of the pair correlation function for large particles, as shown in Fig. 7. However, the trends seen in the distributions of Fig. 6 are not sensitive to small variations of this value. Consider Fig. 6(a) which shows the probability of having N_L neighbors for both species of particles. The two distributions are very similar indicating that the neighborhoods of both large and small reference particles contain similar numbers of large particles. Figure 6(b) shows a similar plot counting the likelihood of having N_S small neighbors for both species. Again we find comparable distributions, showing that the sample is statistically homogeneous and there is no size segregation. The most probable neighborhood [the maximum of the probability distribution $P(N_L, N_S)$] is $N_L=7$, $N_S=10$ for large particles, and $N_L=6$, $N_S=10$ for small particles.

The probability distributions in Fig. 6 do not depend on sample age. This is in agreement with previous work on aging monodisperse glasses where other local measures of structure did not show any aging [10]. However, in that study the structure showed some correlation to the dynamics. To establish whether this still holds in a binary suspension, we first calculate the mobility of each particle. To do this, we choose a fixed lag time $\Delta t=10$ min, and calculate $\Delta r^2(t_w, \Delta t)$ for each particle at each time t_w. The results that follow do
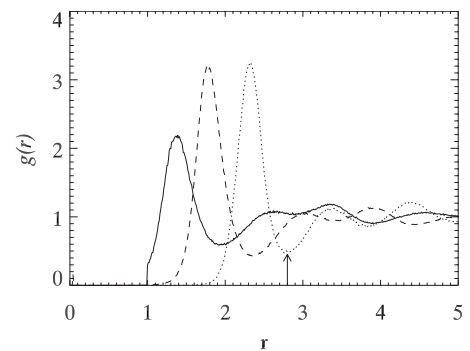

FIG. 7. Pair correlation functions $g_{SS}(r)$ (solid line), $g_{LL}(r)$ (dotted line), and $g_{SL}(r)$ (dashed line). The arrow at $r=2.8$ μm indicates the cutoff used to define nearest neighbors. These functions do not change as the sample ages.
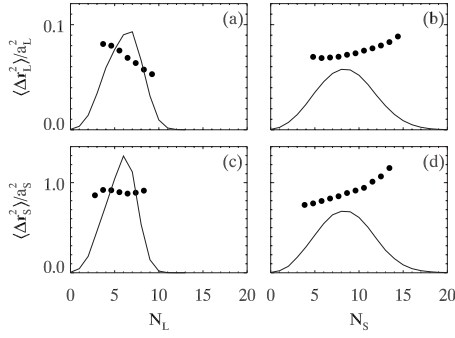
FIG. 8. Average particle mobility versus the number and type of neighbors the particle has (circles) for $\Delta t = 10$ min. The solid line is proportional to the probability of having that number and type of neighbors. (a) Large particles with large neighbors, (b) large particles with small neighbors, (c) small particles with large neighbors, (d) and small particles with small neighbors. The trends in these graphs do not change as the sample ages or with choice of Δt. The curves are truncated where the probabilities of having that many neighbors drops below 3%.

not depend on this choice of Δt. We then average the mobility over all particles of a given size with the same number of large or small neighbors, and plot these results in Fig. 8. We observe that, on average, having more small neighbors allows a reference particle to be more mobile. Conversely, a local environment rich in large neighbors tends to inhibit mobility. This seems to hold whether the reference particle is large or small, as can be seen by comparing the top and bottom rows of Fig. 8. Therefore, in this binary sample, not only are the small particles more mobile on average, but they also facilitate the mobility of their neighbors independently of their size. Of course, this is only true on average; these results vary quite a lot from particle to particle [54].

This is similar to previous observations of binary systems using rheology [28,29] and light scattering [30]. These studies found that binary suspensions have lower viscosities and faster microscopic motion compared to monodisperse samples of equal total volume fraction. This was attributed to the fact that binary suspensions are capable of packing to higher volume fractions; thus at a given volume fraction, there is more free volume for a binary suspension as compared to a monodisperse suspension. In particular, a glassy binary suspension has faster dynamics and can even become liquidlike with a sufficiently high population of small particles [30]. For our experiment, we have purposely chosen the overall volume fraction to ensure that the sample still has glassy behavior. Nonetheless, Fig. 8 shows that the small particles "lubricate" the motion of the large ones, as proposed to interpret the earlier experiments [30].

To further investigate the role the small particles have in the aging of the sample, we examine the distribution of particle displacements over the same lag time of 10 minutes. Figure 9 shows $\langle \Delta x^2(t_w) \rangle$ (solid lines), which is the second moment of the distribution of displacements, as a function of sample age, t_w, for large particles (top) and small particles (bottom). Note that here the angle brackets $\langle \cdots \rangle$ indicate an average over all particles, but not over times t_w. The data decrease, reflecting the slowing of motion already seen in
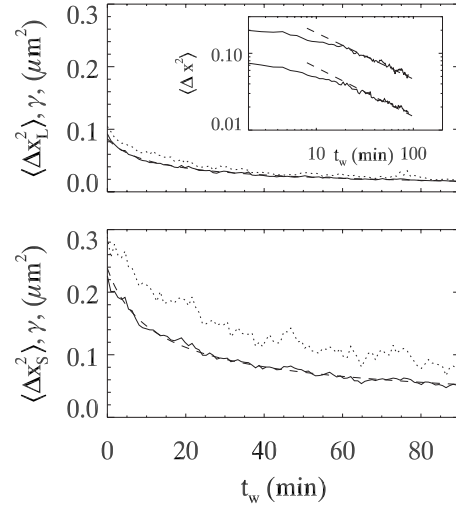

FIG. 9. $\langle \Delta x^2 \rangle$ (solid) and $\gamma = \sqrt{\langle x^4 \rangle / 3}$ (dotted) as a function of sample age for large particles and small particles as indicated. The displacements are defined using $\Delta t = 10$ min. The solid lines are fit to power laws (dashed). Inset: Same data plotted on a log-log plot; the upper line corresponds to the small particles, and the lower line to the large particles.

Fig. 2. The small fluctuations in each graph indicate periods of extra activity (of the sort pictured in Fig. 4), and have been seen previously [14,16,23,55].

The non-Gaussianity of the sample can be determined by comparing these solid curves to the dotted curves, which represent $\gamma = \sqrt{\langle \Delta x^4 \rangle / 3}$. The ratio $\gamma / \langle \Delta x^2 \rangle = 1$ for a Gaussian distribution. In our sample, this ratio is ≈ 1.2 for the large particles and ≈ 1.6 for the small particles. Both of these ratios are greater than 1 indicating that the dynamics are anomalous: There is an excess of large steps when compared to a Gaussian distribution with the same width. This result is typical in a monodisperse dense suspension [33]. Interestingly, this ratio is slightly greater for the small particles, supporting our assertion that the small particles move in an even more heterogeneous way. This suggests that the subset of small particles with unusually high mobilities dominate the dynamics. Note that we use $\Delta t = 10$ min because the experiment includes time scales $t_w \ll \Delta t$, $t_w \sim \Delta t$, and $t_w \gg \Delta t$, and the non-Gaussian behavior of the small particles is present at all of these time scales.

To characterize the slowing of the dynamics, we fit the large t_w decay of $\langle x^2 \rangle (t_w)$ in Fig. 9 to a power-law decay of the form $\langle \Delta x^2 \rangle \sim t^{-b}$ where $b_L = 0.64 \pm 0.05$ for the large particles and $b_S = 0.60 \pm 0.05$ for the small particles; these fits are shown as dashed lines in the figure. The inset of Fig. 9 shows a log-log plot with the same data and highlights the power-law decay at large t_w. We note that it is possible and perhaps likely that this power-law decay is a transient effect that could disappear at substantially longer t_w [40]; for our data, we regard this as simply one way to characterize the behavior. The values of the exponents b vary from experiment to experiment and are in the range of 0.60–0.80 for this sample. Within our uncertainty, the large and small particles decay almost at the same rates, as suggested by the similar shapes of the MSD curves (Fig. 2). However, comparisons

between different data sets always find $b_L > b_S$ by a small amount. A study of aging in a monodisperse colloidal sample found a range of power-law decay exponents of $0.05 < b < 0.5$ [23]. This prior experiment studied colloidal particles with radius $a \approx 1.18$ μm which is intermediate to the particle radii used in our experiment. However, the power-law decay exponent range found in Ref. [23] is less than both exponents found in this study; apparently this binary suspension ages "faster." Given our observations that the smaller particles facilitate the motion of their neighbors, perhaps the presence of these small particles results in this faster aging as compared with Ref. [23].

IV. CONCLUSION

We study aging in a binary colloidal glass using confocal microscopy and distinguish between the small and large particles within the sample. These two particle species slow down with age similarly to each other, but the smaller par-

ticles appear to be more important in the aging process. These small particles are more mobile, more dynamically heterogeneous, and facilitate the motion of other small particles and the motion of the large particles. Furthermore, significant motions within the sample (presumably responsible for the aging) take place in cooperative groups of mobile particles. From a practical viewpoint, these results suggest that the aging of a sample could be influenced by controlling the size ratio and number ratio of the two species. Another likelihood is that a poorly mixed sample would have spatially heterogeneous aging, depending on the local composition.

ACKNOWLEDGMENTS

[1] H. Sillescu, J. Non-Cryst. Solids **243**, 81 (1999).

[2] W. Götze and L. Sjogren, Rep. Prog. Phys. **55**, 241 (1992).

[3] M. D. Ediger, C. A. Angell, and S. R. Nagel, J. Phys. Chem. **100**, 13200 (1996).

[4] K. A. Dawson, Curr. Opin. Colloid Interface Sci. **7**, 218 (2002).

[5] F. H. Stillinger, Science **267**, 1935 (1995).

[6] C. A. Angell, Science **267**, 1924 (1995).

[7] C. A. Angell, K. L. Ngai, G. B. McKenna, P. F. McMillan, and S. W. Martin, J. Appl. Phys. **88**, 3113 (2000).

[8] I. M. Hodge, Science **267**, 1945 (1995).

[9] W. van Megen, T. C. Mortensen, S. R. Williams, and J. Müller, Phys. Rev. E **58**, 6073 (1998).

[10] G. C. Cianci, R. E. Courtland, and E. R. Weeks, AIP Conf. Proc. **832**, 21 (2006).

[11] G. C. Cianci, R. E. Courtland, and E. R. Weeks, Solid State Commun. **139**, 599 (2006).

[12] E. R. Nowak, J. B. Knight, E. Ben-Naim, H. M. Jaeger, and S. R. Nagel, Phys. Rev. E **57**, 1971 (1998).

[13] L. Cipelletti and L. Ramos, Curr. Opin. Colloid Interface Sci. **7**, 228 (2002).

[14] L. Cipelletti, H. Bissig, V. Trappe, P. Ballesta, and S. Mazoyer, J. Phys.: Condens. Matter **15**, S257 (2003).

[15] L. Cipelletti, L. Ramos, S. Manley, E. Pitard, D. A. Weitz, E. E. Pashkovski, and M. Johansson, Faraday Discuss. **123**, 237 (2003).

[16] E. D. Masri, M. Pierno, L. Berthier, and L. Cipelletti, J. Phys.: Condens. Matter **17**, S3543 (2005).

[17] R. Bandyopadhyay, D. Liang, H. Yardimci, D. A. Sessoms, M. A. Borthwick, S. G. J. Mochrie, J. L. Harden, and R. L. Leheny, Phys. Rev. Lett. **93**, 228302 (2004).

[18] S. Jabbari-Farouji, D. Mizuno, M. Atakhorrami, F. C. MacKintosh, C. F. Schmidt, E. Eiser, G. H. Wegdam, and D. Bonn, Phys. Rev. Lett. **98**, 108302 (2007).

[19] M. Bellour, A. Knaebel, J. L. Harden, F. Lequeux, and J. P. Munch, Phys. Rev. E **67**, 031405 (2003).

[20] K. Chen and K. S. Schweizer, Phys. Rev. Lett. **98**, 167802 (2007).

[21] K. L. Ngai, Philos. Mag. **87**, 357 (2007).

[22] P. N. Pusey and W. van Megen, Nature (London) **320**, 340 (1986).

[23] R. E. Courtland and E. R. Weeks, J. Phys.: Condens. Matter **15**, S359 (2003).

[24] W. K. Kegel, Langmuir **16**, 939 (2000).

[25] H. J. Schope, G. Bryant, and W. van Megen, J. Chem. Phys. **127**, 084505 (2007).

[26] W. Kob and J.-L. Barrat, Phys. Rev. Lett. **78**, 4581 (1997).

[27] W. Kob, J.-L. Barrat, F. Sciortino, and P. Tartaglia, J. Phys.: Condens. Matter **12**, 6385 (2000).

[28] R. L. Hoffman, J. Rheol. **36**, 947 (1992).

[29] P. D'Haene and J. Mewis, Rheol. Acta **33**, 165 (1994).

[30] S. R. Williams and W. van Megen, Phys. Rev. E **64**, 041502 (2001).

[31] A. D. Dinsmore, E. R. Weeks, V. Prasad, A. C. Levitt, and D. A. Weitz, Appl. Opt. **40**, 4152 (2001).

[32] L. Antl, J. W. Goodwin, R. D. Hill, R. H. Ottewill, S. M. Owens, S. Papworth, and J. A. Waters, Colloids Surf. **17**, 67 (1986).

[33] E. R. Weeks, J. C. Crocker, A. C. Levitt, A. Schofield, and D. A. Weitz, Science **287**, 627 (2000).

[34] S. I. Henderson, T. C. Mortensen, S. M. Underwood, and W. van Megen, Physica A **233**, 102 (1996).

[35] S. Auer and D. Frenkel, Nature (London) **413**, 711 (2001).

[36] J. M. G. Cowie and R. Ferguson, Macromolecules **22**, 2312 (1989).

[37] I. M. G. Cowie, V. Arrighi, and E.-A. Mcgonigle, Macromol. Chem. Phys. **206**, 767 (2005).

[38] V. Prasad, D. Semwogerere, and E. R. Weeks, J. Phys.: Condens. Matter **19**, 113102 (2007).

[39] J. C. Crocker and D. G. Grier, J. Colloid Interface Sci. **179**,

298 (1996).

[40] G. B. McKenna, J. Phys.: Condens. Matter **15**, S737 (2003).

[41] M. Cloitre, R. Borrega, and L. Leibler, Phys. Rev. Lett. **85**, 4819 (2000).

[42] D. Bonn, S. Tanase, B. Abou, H. Tanaka, and J. Meunier, Phys. Rev. Lett. **89**, 015701 (2002).

[43] V. Viasnoff and F. Lequeux, Phys. Rev. Lett. **89**, 065701 (2002).

[44] E. R. Weeks and D. A. Weitz, Phys. Rev. Lett. **89**, 095704 (2002).

[45] W. K. Kegel and A. van Blaaderen, Science **287**, 290 (2000).

[46] C. Donati, J. F. Douglas, W. Kob, S. J. Plimpton, P. H. Poole, and S. C. Glotzer, Phys. Rev. Lett. **80**, 2338 (1998).

[47] A. Widmer-Cooper, P. Harrowell, and H. Fynewever, Phys.

[48] H. Sillescu, R. Bohmer, G. Diezemann, and G. Hinze, J. Non-Cryst. Solids **307-310**, 16 (2002).

[49] L. Berthier, Phys. Rev. E **69**, 020201(R) (2004).

[50] R. Yamamoto and A. Onuki, Phys. Rev. E **58**, 3515 (1998).

[51] M. D. Ediger, Annu. Rev. Phys. Chem. **51**, 99 (2000).

[52] A. Mehta, G. C. Barker, and J. M. Luck, Proc. Natl. Acad. Sci. U.S.A. **105**, 8244 (2008).

[53] D. I. Goldman and H. L. Swinney, Phys. Rev. Lett. **96**, 145702 (2006).

[54] J. C. Conrad, F. W. Starr, and D. A. Weitz, J. Phys. Chem. B **109**, 21235 (2005).

[55] H. E. Castillo and A. Parsaeian, Nat. Phys. **3**, 26 (2007).

Rev. Lett. **93**, 135701 (2004).